processes

Article

Determining the Bimodal Soil–Water Characteristic Curve of Fine-Grained Subgrade Soil Derived from the Compaction Condition by Incorporating Pore Size Distribution

Xinran Chen [1], Minglei Ma [1,*], Shumei Zhou [1], Mingjun Hu [2], Jianmin Ma [3] and Sen Wei [1]

1 China Construction Eighth Engineering Division Co., Ltd., 1568 Century Avenue, Shanghai 200122, China
2 School of Transportation and Logistics, Dalian University of Technology, Dalian 116024, China
3 Department of Chemistry, Queen's University, Kingston, ON K7L 3N6, Canada; jianmin.ma@queensu.ca
* Correspondence: minglei_m@163.com

Abstract: The soil–water characteristic curve (SWCC) is a key constitutive relationship for unsaturated soil which can be unimodal or bimodal. For the fine-grained compacted subgrade soil with a bimodal pattern, the determination of SWCC is complicated and needs a wide-range suction measurement. In this paper, the bimodal SWCC of a subgrade soil derived from the compaction condition was measured and determined by incorporating pore size distribution. For this purpose, a series of laboratory tests were conducted, including the pressure plate method, filter paper method, and vapor equilibrium method, which were used to measure SWCC at the low, medium, and high suction range, respectively. The pore size distribution (PSD) data were obtained by mercury intrusion porosimetry (MIP) tests and used to predict SWCC. Based on the analysis of hydraulic paths and SWCC-PSD correlations, the SWCC of the subgrade soil should be determined to follow the actual hydraulic path. SWCC within a low suction range can be filled by PSD-based data to improve the fitting accuracy. Then, a graphical method is applied to predict the bimodal SWCC by combining the filter paper method, vapor equilibrium method, and PSD-based data. The prediction curves fit well with the test data for all selected compaction conditions. Furthermore, the prediction method can still provide good prediction performance in the absence of high suction section data, which is beneficial for the application of bimodal SWCC.

Keywords: unsaturated soil; soil–water characteristic curve; matric suction; pore size distribution

Citation: Chen, X.; Ma, M.; Zhou, S.; Hu, M.; Ma, J.; Wei, S. Determining the Bimodal Soil–Water Characteristic Curve of Fine-Grained Subgrade Soil Derived from the Compaction Condition by Incorporating Pore Size Distribution. *Processes* **2023**, *11*, 3394. https://doi.org/10.3390/pr11123394

Academic Editors: Haiping Zhu and Kejun Dong

Received: 7 November 2023
Revised: 3 December 2023
Accepted: 7 December 2023
Published: 9 December 2023

1. Introduction

The soil–water characteristic curve (SWCC) is an essential relationship between soil suction and water content in unsaturated soils [1,2]. Besides the water retention capacity, SWCC could be used to investigate and predict several geotechnical properties of unsaturated soils, including the unsaturated shear strength [3–7], stress–strain relationship [8,9] and unsaturated permeability [10–12]. The SWCC of soils with different soil types and particle characteristics differs significantly. With the continuous investigation of SWCC, many studies have found that the SWCC of a particular soil is not a unique curve, but is generally affected by many factors, such as the compaction conditions, void ratios, hydraulic paths and temperature of soils.

Due to the importance of SWCC, several measurement methods were developed, and the test data was used to determine mathematical SWCC models. Early researchers believed that the SWCC was a unimodal "s" shaped curve, and several SWCC prediction models were proposed following this shape, such as the widely used Brooks and Corey model [13], Van Genuchten model [14] and Fredlund and Xing model [15]. The parameters of these models were commonly obtained by the optimization method, with the error minimized by iterating the parameters [2,16,17]. To quantitively reflect the influence factors of SWCC, the latest studies tend to estimate the unimodal SWCC for the soil with different initial void ratios using a single fitting function [18].

With the development of microstructure detection methods, the mercury intrusion porosimetry (MIP), scanning electronic microscope (SEM) and X-ray diffraction methods provide a direct way to investigate the pore structure of unsaturated soils. It was found that some soil types have bimodal pore structures, which can be divided into inter-aggregate pores and intra-aggregate pores. The pore water in the soil with bimodal pore structures can also be divided into capillary water and adsorbed water. The capillary water in the inter-aggregate pores is easy to exclude, and the adsorbed water in the intra-aggregate pores tends to be trapped in the pores. Thus, the soil with bimodal pore structures suggests a double "s" shape bimodal SWCC [19]. Compared with unimodal SWCC, the determination of bimodal SWCC generally needs a set of test data over a wider suction range, which is time-consuming and expensive. In addition, new mathematical models are required to determine bimodal SWCC. The generally adopted approach to build a bimodal SWCC prediction model was separating the bimodal SWCC into two unimodal SWCC corresponding to the inter-aggregate pores and intra-aggregate pores in the soil, and then the two unimodal SWCC were fitted, respectively [20–22]. The selection of the intersection point and the number of fitting parameters would significantly affect the fitting difficulty [23]. In addition, the accuracy of the test data at the intersection point significantly affects the accuracy of the entire bimodal SWCC.

To reduce the fitting uncertainty of the bimodal SWCC, several researchers intended to reduce the number of fitting parameters in the prediction model [19,24,25]. Gitirana and Fredlund [26] and Satyanaga et al. [19] used the measured water content and matric suction at the intersection point of the two curves as the fixed point of SWCC and required only one or two additional fitting parameters. Othmer et al. [27], Mallants et al. [28] and Zhang and Chen [29] built continuous bimodal SWCC models using the superposition of two fitting functions, but all parameters need to be fitted at the same time, which may cause fitting failure.

Due to the difficulty and uncertainty in bimodal SWCC fitting, several researchers tried to find indirect ways to determine SWCC. For example, Ren et al. [30] and Atma et al. [31] built SWCC models using experimental data over a limited suction range, and the model performed well in predicting the unimodal SWCC. Zhai et al. [32] and Chai and Khaimook [33] used grain-size distribution (GSD) of soils to predict SWCC, and it was found that the SWCC-GSD relationship is affected by the pore structures [19,34]. The mercury intrusion porosimeter (MIP) test has been widely employed to obtain quantitative information on the pore structure, and the pore size distribution (PSD) data could also be used for predicting SWCC [35–38]. However, the accuracy of PSD is not sufficient for determining the entire SWCC due to the test error and size effect [39].

In this paper, the bimodal SWCC was determined by a continuous model incorporating PSD data. A fine-grained subgrade soil was used as the test material. Three different laboratory test methods were adopted to measure SWCC, and the PSD curves obtained by MIP tests were also used to calculate SWCC. Considering the hydraulic path of subgrade soil after compaction, the bimodal SWCC derived from the compaction condition was determined by incorporating PSD data, and its efficiency was verified under nine different compaction conditions.

2. Materials and Experimental Methods

2.1. Material

The tested subgrade soil was a granite-residual soil from Jiangxi, China, and its grain-size distribution is presented in Figure 1a. The soil had a plastic limit of 22% and a liquid limit of 62% and was classified as high-liquid limit clay based on the Unified Soil Classification System. The specific gravity of the soil was 2.74. The chemical analysis showed that the soil was composed of quartz, kaolinite, gibbsite, chlorite and iron-rich minerals. Therefore, the mechanical properties of the soil would be sensitive to moisture change.

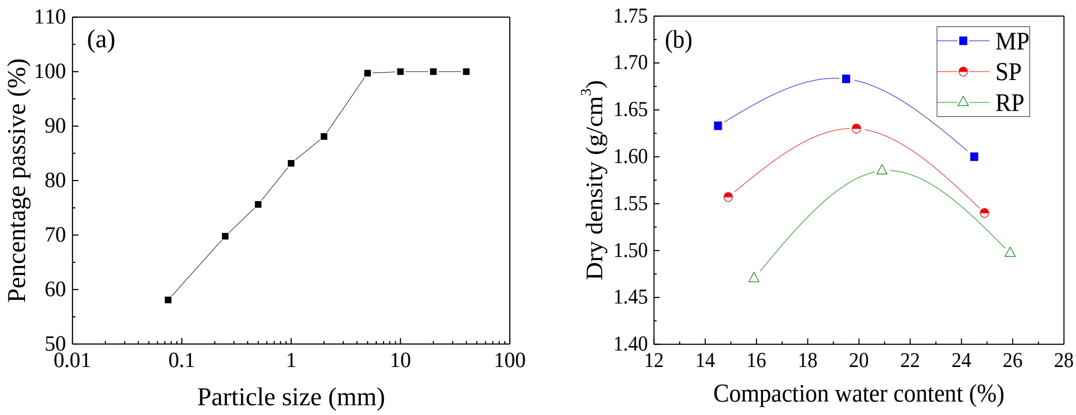

Figure 1. Material properties of the tested soil: (**a**) grain-size distribution and (**b**) proctor curves.

2.2. Sample Preparation

The soil samples were prepared using different compaction water contents and compaction efforts based on the proctor curves to simulate the variation in compaction conditions of the subgrade soil, as presented in Figure 1b. Three compaction water contents were selected around the optimum moisture content (OMC), which were OMC −5%, OMC and OMC +5%. Then, the soil samples were compacted according to the JTG 3430-2020 [40] standard. A compaction effort of 2677.2 kJ/m^3 was applied 98, 50 and 30 blows per layer, named modified proctor (MP), standard proctor (SP), and reduced proctor (RP). Then, the tested soil was air-dried naturally, passed through 2 mm sieves, and statically compacted to the target compaction conditions. The compaction water content and dry density of all samples are summarized in Table 1.

Table 1. Selected compaction conditions corresponding to proctor curves.

Proctor Type	MP	MP	MP	SP	SP	SP	RP	RP	RP
Water content refers to OMC	−5%	+0%	+5%	−5%	+0%	+5%	−5%	+0%	+5%
Compaction water content (%)	14.5	19.5	24.5	14.9	19.9	24.9	15.9	20.9	25.9
Dry density (g/cm^3)	1.63	1.68	1.60	1.56	1.63	1.54	1.47	1.58	1.50

2.3. Laboratory Test Methods

To obtain SWCC over a wide suction range, the pressure plate method, filter paper method and vapor equilibrium method were used for different suction ranges. Also, MIP tests were conducted to obtain the pore size distribution of soil samples and to predict SWCC. All tests were conducted in a temperature-controlled room at 20 °C.

2.3.1. Pressure Plate Method

The axis-translation technique was suitable for measuring the SWCC of soils at a suction under 1500 kPa [41,42]. In this paper, the Geo-experts stress-related pressure plate device was adopted via this technique with 15-bar high air entry ceramic discs, as shown in Figure 2a. Following ASTM-D6836-16 [43] standard procedure method B, the tested soil was compacted in a cutting ring with a diameter of 6.18 cm and a height of 2 cm, vacuum saturated (Figure 2b), and put into a closed pressure chamber. Then, a suction sequence of 10, 20, 40, 70, 100, 200, 400 and 600 (kPa) was applied for desaturation under zero vertical stress. For each suction level, the suction was held constant until the moisture equilibrium was reached. After that, the sample was taken out to measure its residual water content. By recording the amount of water out of the soil sample corresponding to each suction level, the relationship between suction and water content could be calculated, and the SWCC was obtained. The saturated water content was tested separately by the oven-drying method.

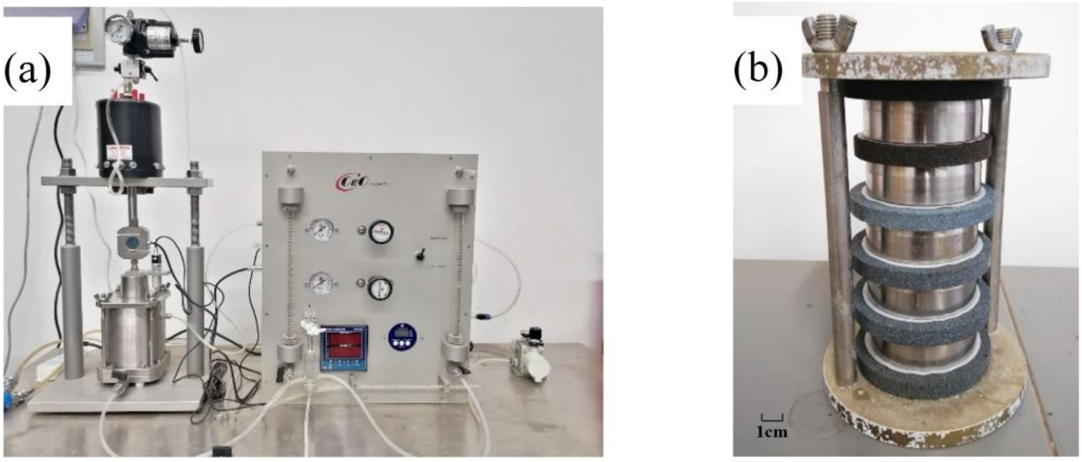

Figure 2. (**a**) The pressure plate device and (**b**) the vacuum saturation fixture.

2.3.2. Filter Paper Method

The filter paper method was used for measuring the SWCC of the tested soil samples for the matric suction ranging from 1000 to 10,000 kPa following ASTM D5298-16 testing protocols [44]. Whatman No. 42 filter papers with a diameter of 4.5 cm were used in this paper. To obtain the SWCC derived from the compaction condition, the samples were compacted in a cutting ring at the selected condition and then wetted or air-dried to 8 different water contents around the optimum moisture content, which were OMC −11.5%, −9.5%, −7.5%, −5%, −2.5%, −0%, +2.5% and +5%. The filter paper used for suction measurement was sandwiched between two protective filter papers and put under the compacted soil sample, as depicted in Figure 3a. Then, the sample and filter paper were placed in a sealed box for two weeks for moisture equilibrium, as shown in Figure 3b. At the end of two weeks, the filter paper was retrieved, and its water content (w_{fp}) was measured with an electronic scale with an accuracy of 0.0001 g. The calibration curve between w_{fp} and matric suction s of soils is expressed in Equation (1), according to ASTM D5298-16 [44]:

$$\lg s = \begin{cases} -0.0779 w_{fp} + 5.327, w_{fp} < 45.264 \\ -0.0135 w_{fp} + 2.412, w_{fp} \geq 45.264 \end{cases} \quad (1)$$

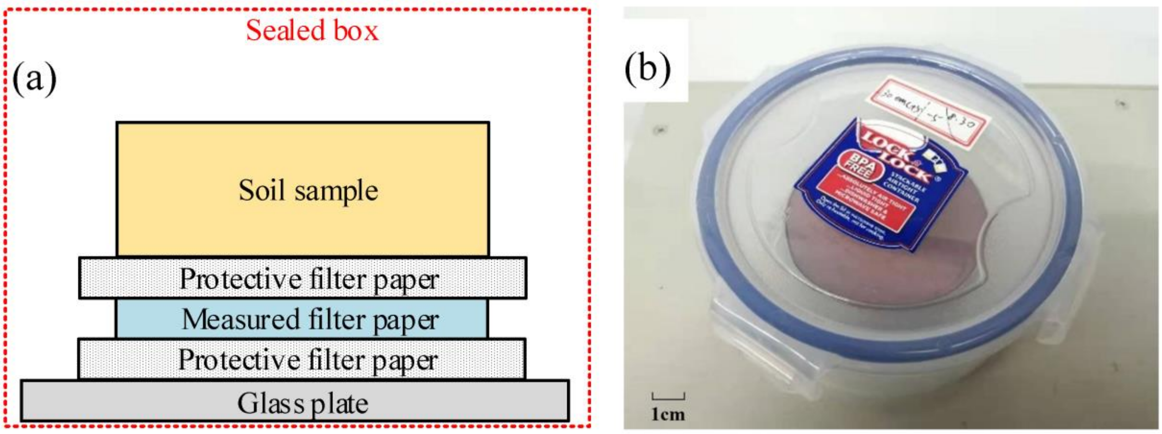

Figure 3. Placement of the filter paper method: (**a**) The schematic diagram and (**b**) the sealed box with sample inside.

2.3.3. Vapor Equilibrium Method

For the high suction range above 10,000 kPa, the vapor equilibrium method was commonly used [45–47]. This method is based on the unique relationship between the relative humidity (RH) and the spatial vapor pressure in a closed space. The total suction of the soil sample in the space is equal to the spatial vapor pressure and can be controlled by chemical solutions with different concentrations and relative humidity. The supersaturated salt solutions were used to provide constant relative humidity values in this paper [45,47]. The soil samples inside the closed space would be dried by moisture exchange between the vapor and liquid phases until the suction equilibrium was reached.

Considering the required suction range of SWCC tests, five commonly used salts were selected, which were $ZnSO_4$, NaCl, NaBr, $MgCl_2$ and LiCl. These saturated salt solutions provided suction ranging from 12.6 MPa to 286.7 MPa at 20 °C, as shown in Table 2.

Table 2. Suction and relative humidity of saturated salt solutions.

Saturated Salt Solution	$ZnSO_4$	NaCl	NaBr	$MgCl_2$	LiCl
RH (%)	89.96	75.47	59.1	33.1	12.0
Total suction (MPa)	12.6	38	71.12	149.51	286.7

A sealed desiccator with a porous disk was used to provide closed space with a supersaturated salt solution at the bottom, as shown in Figure 4a. The cylindrical soil samples with a diameter of 1 cm and a height of 1 cm were prepared and placed into a glass beaker and suspended above the porous disk, as shown in Figure 4b. According to related research, the samples were placed in the sealed desiccators for 30 days to reach the vapor equilibrium [46–48]. After that, the change in water content in the sample was measured and calculated to obtain the corresponding SWCC data.

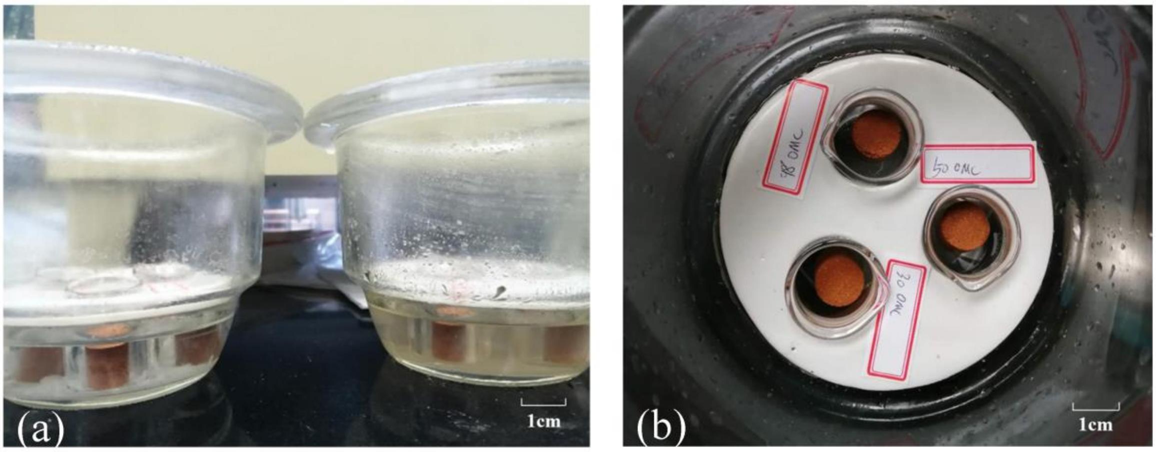

Figure 4. (**a**) The sealed desiccators containing supersaturated salt solutions and (**b**) the placement of soil samples.

2.3.4. Mercury Intrusion Porosimetry Test

To obtain the pore size distribution of tested soil samples, the commonly used mercury intrusion porosimetry (MIP) test was adopted [35,36,49]. Micromeritics AutoPore IV 9510 (Atlanta, GA, USA) with a maximum intrusion pressure of 60,000 psia (414 MPa) was used to conduct MIP tests in this paper. As shown in Figure 5, the soil sample was compacted in the cutting ring first and cut into 1 cm^3 cube to fit the dilatometer size. The cubes were then freeze-dried at −50 °C for 24 h to remove the pore moisture with minimal disturbance on the pore structure [35,37].

Figure 5. (**a**) The compacted sample, (**b**) cutting the sample to a 1 cm^3 cube, (**c**) freeze-drying and (**d**) the MIP test device.

To operate the test, the sealed dilatometer with dried cubes inside was placed in the low-pressure and high-pressure port successively. During this process, the air in the soil was replaced by mercury with increasing intrusion pressure, and the pore diameters (d) were continuously recorded during the test. Thus, the pore size distribution of soil samples could be obtained for analysis.

3. Results and Discussions

3.1. SWCC Results from Different Measurement Methods

The measured SWCC obtained by the pressure plate method, filter paper method and vapor equilibrium method are depicted in Figure 6. The typical "s" shape curve is shown for all the nine compaction conditions. The data from the filter paper method and vapor equilibrium method shows good consistency. On the contrary, discontinuity was observed between the pressure plate method and the filter paper method in most cases. Thus, SWCC will be significantly affected by the set of test data used for curve fitting, which also causes uncertainty in SWCC determination.

3.2. Analysis of the Hydraulic Path for the Subgrade Soil

The difference in test data obtained by different test methods can be analyzed based on the tested hydraulic path. It is well known that the SWCC of unsaturated soil is dependent on the hydraulic paths, as shown in Figure 7a. The SWCC of a certain soil sample is enveloped by the main wetting and drying curves, and a change in hydraulic path for a certain suction will change the subsequent SWCC to the scanning curves [50,51]. This phenomenon is due to the difference in contact angles between the wetting and drying path, the ink-bottle effect, and the air entrapment in the pores [52–54].

For the unsaturated subgrade soil, the compaction condition determines the initial matric suction and degree of saturation, and subsequent changes in matric suction due to environmental factors are derived from this condition. Therefore, the SWCC of unsaturated subgrade soil derived from the compaction condition is not an entire wetting or drying curve [55], as depicted in Figure 7b. For the suction higher than the initial value, the SWCC of the subgrade soil belongs to a drying path, while for a suction lower than the initial value, the SWCC belongs to a wetting path. Using the main drying or main wetting curve to predict the water retention capacity of the subgrade soil is inaccurate.

As shown in Figure 8, for the filter paper method and vapor equilibrium method, the tested hydraulic path is the same as the actual hydraulic path of the subgrade soil shown in Figure 7b. By contrast, for the pressure plate method, the pre-test saturation step belongs to the wetting path, and the dewatering step belongs to the drying path, which is different from Figure 7b. Therefore, the measured SWCC data from the pressure plate test was different from the SWCC of subgrade soil derived from the compaction condition.

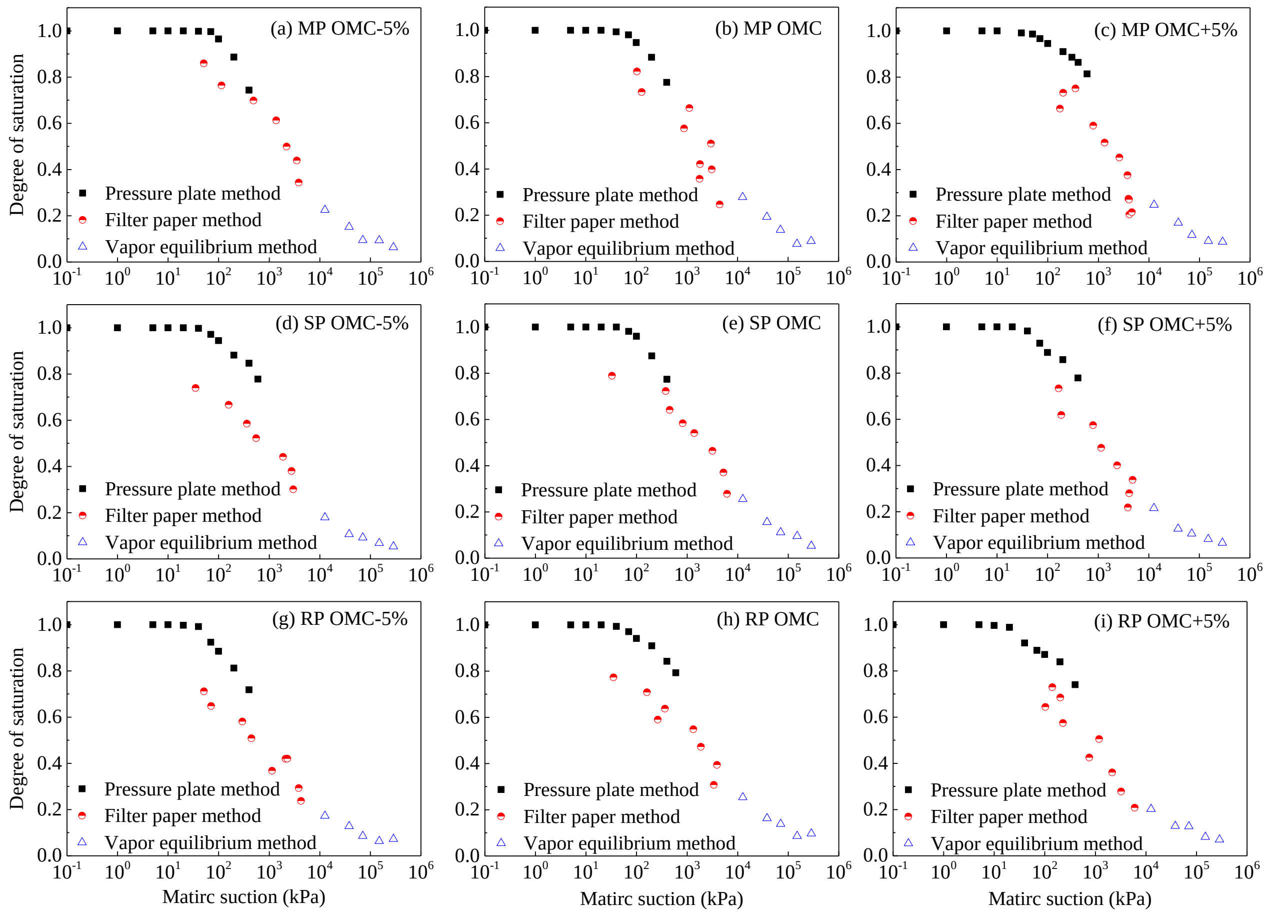

Figure 6. Measured SWCC data from different test methods.

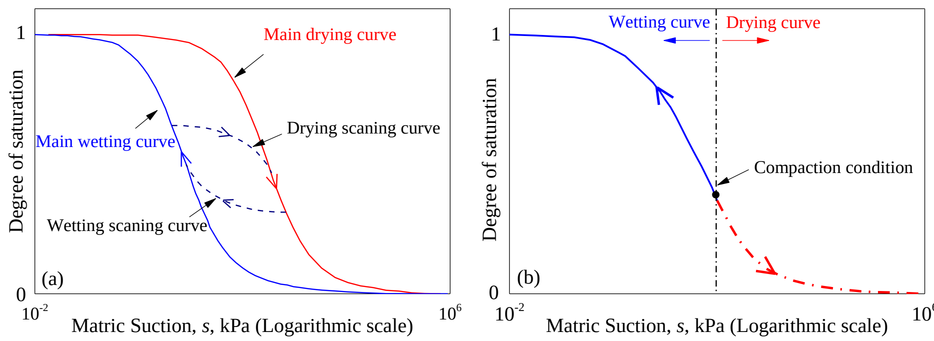

Figure 7. (**a**) The dependence of SWCC on the hydraulic path and (**b**) the actual hydraulic path for SWCC derived from a certain compaction condition.

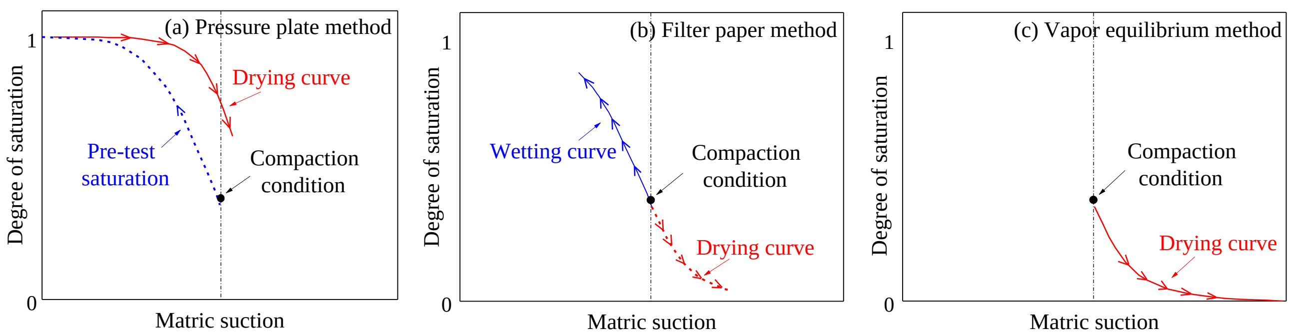

Figure 8. The hydraulic path of SWCC obtained by different tests.

3.3. Correlation between Measured SWCC and Pore Size Distribution Curve

Besides the hydraulic path, the well-accepted correlation between the SWCC and PSD curve was induced for analysis, as theoretically depicted in Figure 9a [56–58]. The matric suction corresponding to the peak value of the PSD curve is consistent with the maximum slope of SWCC, which means that the moisture content changes in the diameter range where pores are concentrated. In order to compare the PSD with measured SWCC in this paper, matric suction corresponding to PSD is calculated using the Young–Laplace equation, as shown by Equation (2).

$$p_{int} = -\frac{4T_{HG}\cos\theta_{HG}}{d} \tag{2}$$

where p_{int} is the intrusion pressure, d is the pore diameter, T_{HG} is the surface tension of mercury (i.e., 0.485 N/m at 20 °C); θ_{HG} is the contact angle between mercury and soil interface (i.e., 141.3°).

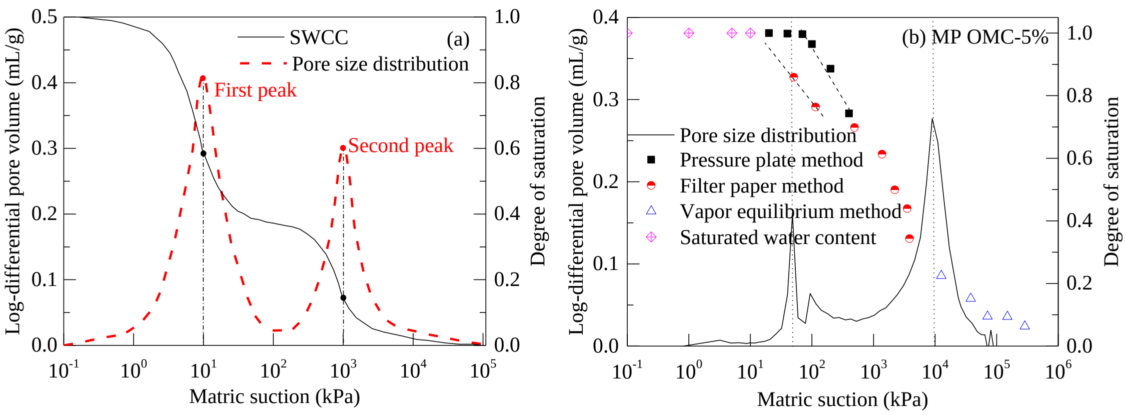

Figure 9. (**a**) Conceptional relationship between bimodal SWCC and PSD curves and (**b**) typical comparison of tested data and PSD curve.

For water in the unsaturated soil, a similar relationship exists for matric suction s and pore diameter d, as shown by Equation (3).

$$s = \frac{4T_w\cos\theta_w}{d} \tag{3}$$

where T_w is the surface tension of water (i.e., 0.0728 N/m at 20 °C); θ_w is the contact angle between water and soil interface (i.e., assumed to be equal to 180°).

Therefore, the relationship between intrusion pressure and matric suction could be described by Equation (4).

$$s = -\frac{T_w\cos\theta_w}{T_{HG}\cos\theta_{HG}}p_{int} \tag{4}$$

The typical comparison of PSD and measured SWCC is depicted in Figure 9b, taking MP OMC −5% as an example. The first peak of PSD curves (i.e., the peak corresponding to inter-aggregate pores) is not continuous with the fast dewatering stage of the test data from the pressure plate method. By contrast, the fast dewatering stage of the test data obtained by the filter paper method and measured saturated water content is consistent with the first peak of PSD curves, which is more reasonable. Therefore, to obtain the SWCC of the subgrade soil following the actual hydraulic path, the measurement methods should follow the same hydraulic path.

3.4. Comparison of Measured and PSD-Based SWCC

Without the pressure plate method, the test data from the filter paper method and saturated water content test cannot precisely determine the shape of SWCC in the low suction range. Thus, the relationship between PSD and SWCC is further investigated. Previous studies indicated that the MIP test is believed to be accurate in the low and medium suction range (i.e., medium and large pores) and is used in related studies to determine the air-entry value of SWCC [39]. Therefore, the SWCC predicted by PSD is calculated and used to fill the measured SWCC data at a low suction range.

The process of mercury intrusion in the MIP test is similar to the process of air intrusion into an initially saturated soil specimen [57,58]. Due to the surface tension, the mercury is subjected to a certain external pressure when it enters a small pore. Thus, under a certain external pressure, the pores smaller than the diameter corresponding to this pressure are all assumed saturated by water. Based on this theory, the degree of saturation based on MIP tests ($S_{r,M}$) is calculated using Equation (5). Combining this with the correlation of matric suction and external pressure calculated by Equation (4), the PSD-based SWCC is obtained.

$$S_{r,M}(d) = \frac{V_t - V_d}{V_t} \times 100\% \tag{5}$$

where V_d is the cumulative intruded volume corresponding to a pore diameter d, and V_t is the total intruded pore volume, which equals the maximum value of the cumulative intruded volume.

Figure 10 shows the comparison of the PSD-based SWCC with the laboratory SWCC data measured by the filter paper method and vapor equilibrium method. The measured SWCC was close to the PSD-based SWCC at the low suction range of 0–1000 kPa, which indicates that PSD-based SWCC within this range can be used to determine the bimodal SWCC. As the matric suction increases, the PSD-based SWCC is higher than the measured SWCC within a suction range of 1000–10,000 kPa and is lower than the measured SWCC for a suction range higher than 10,000 kPa. This is because the non-intruded pores, either too small or isolated, cannot be detected in MIP tests [35,36,59].

3.5. Determination of the Bimodal SWCC Incorporating PSD Data

Based on the observation in Figure 10, a new bimodal SWCC determination method of unsaturated subgrade soil derived from the compaction condition is proposed, which combines the PSD-based SWCC in a suction range corresponding to inter-aggregate pores and the measured SWCC for a medium and high suction range, as shown in Figure 11. To obtain a mathematical expression, the graphically fitting method proposed by Li et al. [25] is used in this paper, as shown in Equation (6). Compared with the segmented fitting method, the unified description of the bimodal SWCC can benefit from further applications, such as predicting the unsaturated shear strength or the hydraulic conductivity curve.

$$\begin{aligned} S_r(s) = {} & \frac{(0.75S_{r,sat} - 3S_{r,R})\sqrt{s_{a1}s_{R1}}^{2/\log(s_{R1}/s_{a1})}}{s^{2/\log(s_{R1}/s_{a1})} + \sqrt{s_{a1}s_{R1}}^{2/\log(s_{R1}/s_{a1})}} + \frac{(0.25S_{r,sat} - S_{r,R})(4s_{R1})^{0.8}}{s^{0.8} + (4s_{R1})^{0.8}} \\ & + \frac{3S_{r,R}\sqrt{s_{a2}s_{R2}}^{2/\log(s_{R2}/s_{a2})}}{s^{2/\log(s_{R2}/s_{a2})} + \sqrt{s_{a2}s_{R2}}^{2/\log(s_{R2}/s_{a2})}} + \frac{S_{r,R}(4s_{R2})^{0.8}}{s^{0.8} + (4s_{R2})^{0.8}} \end{aligned} \tag{6}$$

where $S_{r,sat}$ is the degree of saturation for the saturated condition; $S_{r,R}$ is the residual degree of saturation; s_{a1} and s_{a2} are the air entry value of inter-aggregate pores and intra-aggregate pores, respectively; s_{R1} and s_{R2} are the residual suction of inter-aggregate pores and intra-aggregate pores, respectively.

The determination of the parameters in Equation (6) is presented in Figure 12. It can be seen that the shape of bimodal SWCC is mainly controlled by the coordinate values of four turning points, named 1st to 4th turning points. These turning points are determined by different test methods used in this paper: the 1st turning point is determined using PSD-based SWCC data, the 2nd turning point is determined by combining PSD and filter paper method, the 3rd turning point is only determined using filter paper method, and the 4th turning point is obtained using test data from vapor equilibrium method.

The predicted SWCC of tested soil under nine compaction conditions is shown in Figure 11 by the solid curves. For all compaction conditions, the prediction curves show good agreement with the test data, indicating that the proposed method is reliable. Note that the high suction value range of SWCC, generally over 10,000 kPa, is nearly straight; this part of SWCC could be determined simply. It can be seen in Figure 9b that the suction value around 10,000 kPa corresponds to the second peak of the PSD curve (i.e., the peak corresponding to intra-aggregate pores). This correlation was also observed in related research investigating the PSD and SWCC of the fine-grained clay [60,61]. Therefore, the PSD-based SWCC data around this suction value could be used to replace the test data of the vapor equilibrium method. It can be observed in Figure 10 that the measured SWCC and PSD-based SWCC intersect around the suction value of 10,000 kPa, which can also be seen in related studies [61,62]. Thus, a simple prediction curve can be further obtained using PSD curves and the test data of the filter paper method. Considering the formation of Equation (6), the data point from PSD-based SWCC at the second peak of the PSD curve can be used as the 4th turning point in the bimodal SWCC prediction model.

As shown in Figure 13 by the dashed line, by removing the data from the vapor equilibrium method, the SWCC can still be determined with similar R^2 values in Figure 11. This method could be beneficial for the application of bimodal SWCC since the measurement of SWCC over a high suction range is time consuming [30].

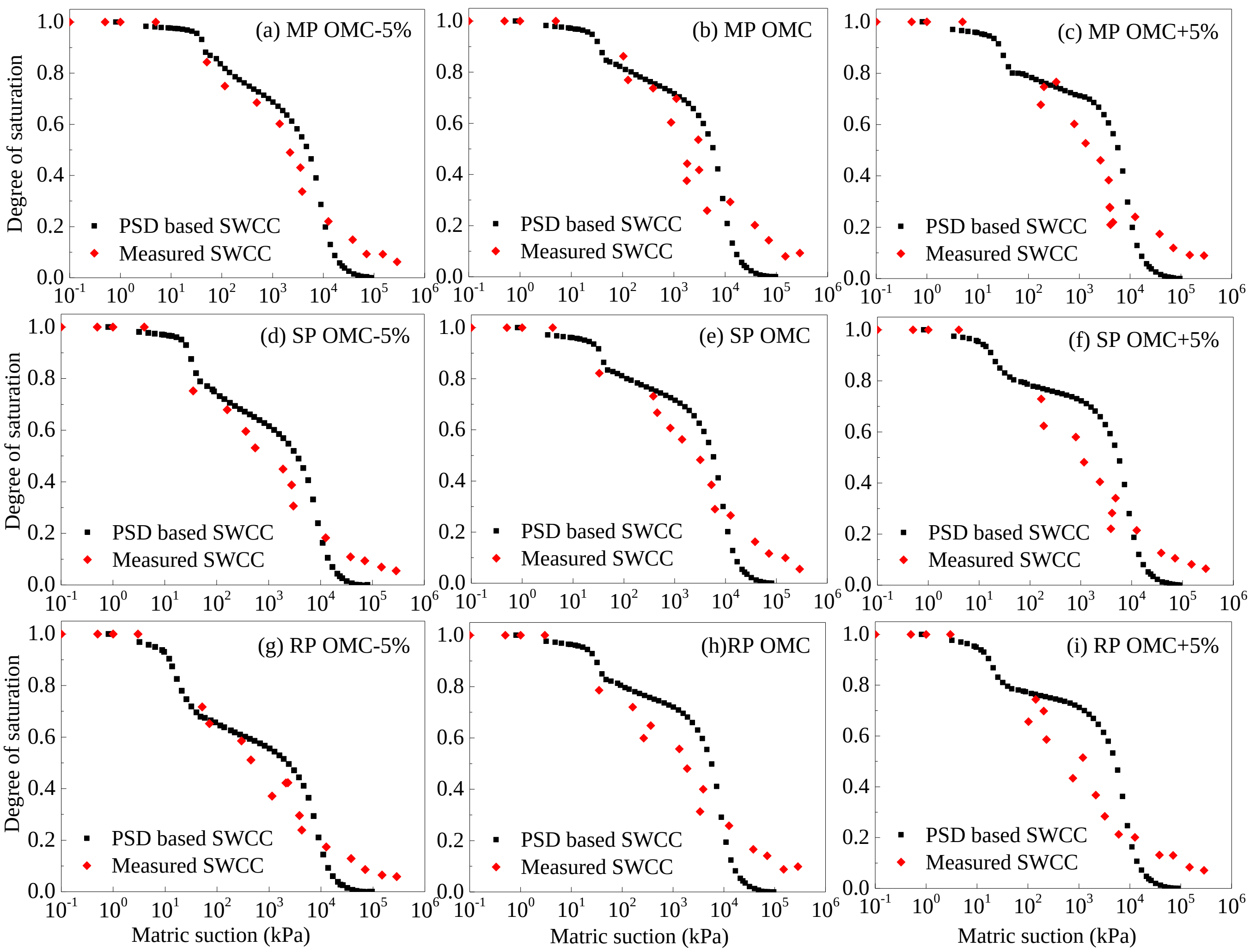

Figure 10. Comparison of PSD-based SWCC and measured SWCC from the filter paper method and vapor equilibrium method.

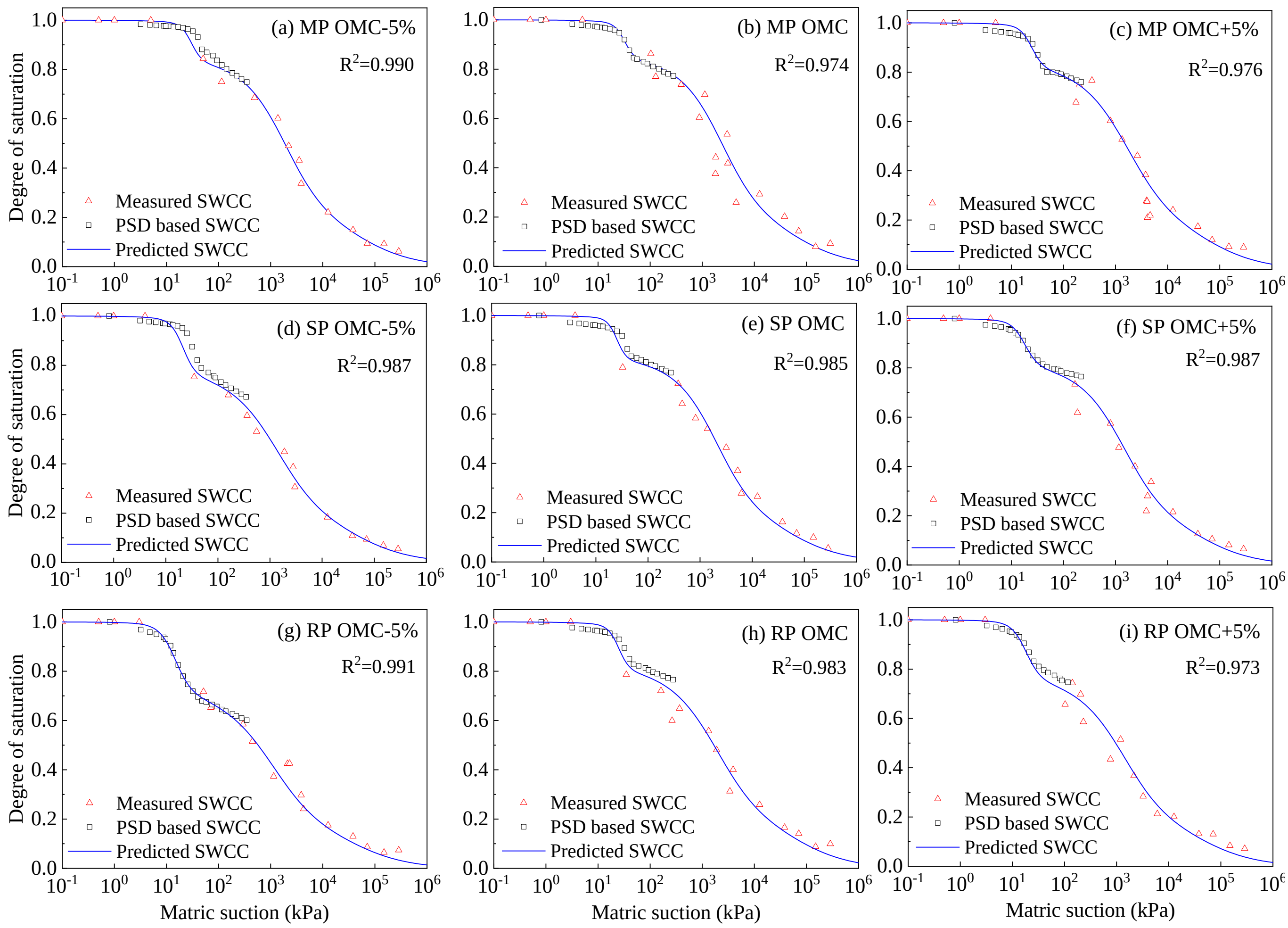

Figure 11. Prediction curves of bimodal SWCC.

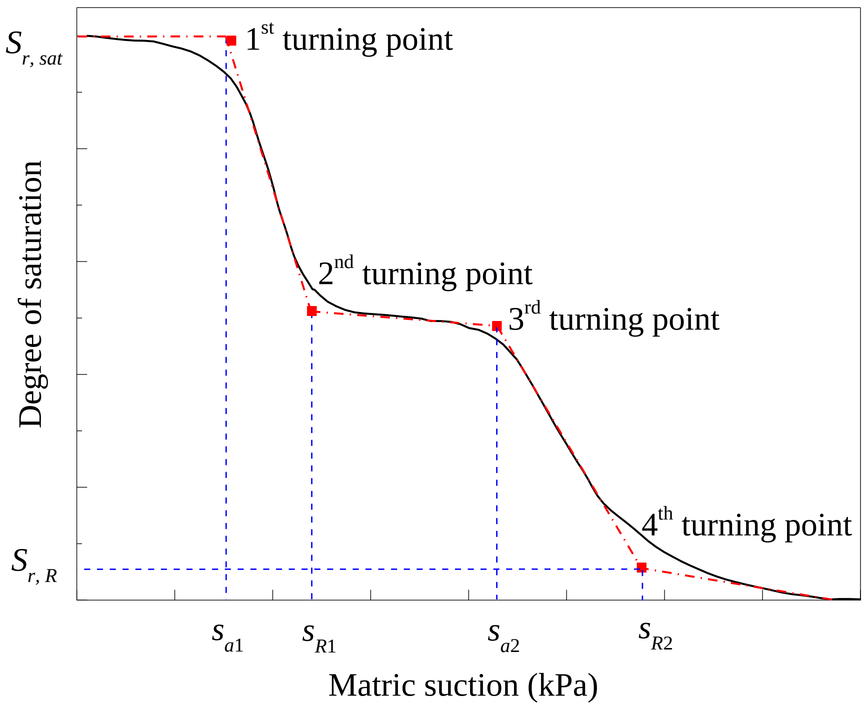

Figure 12. Determination of the parameters for predicting bimodal SWCC.

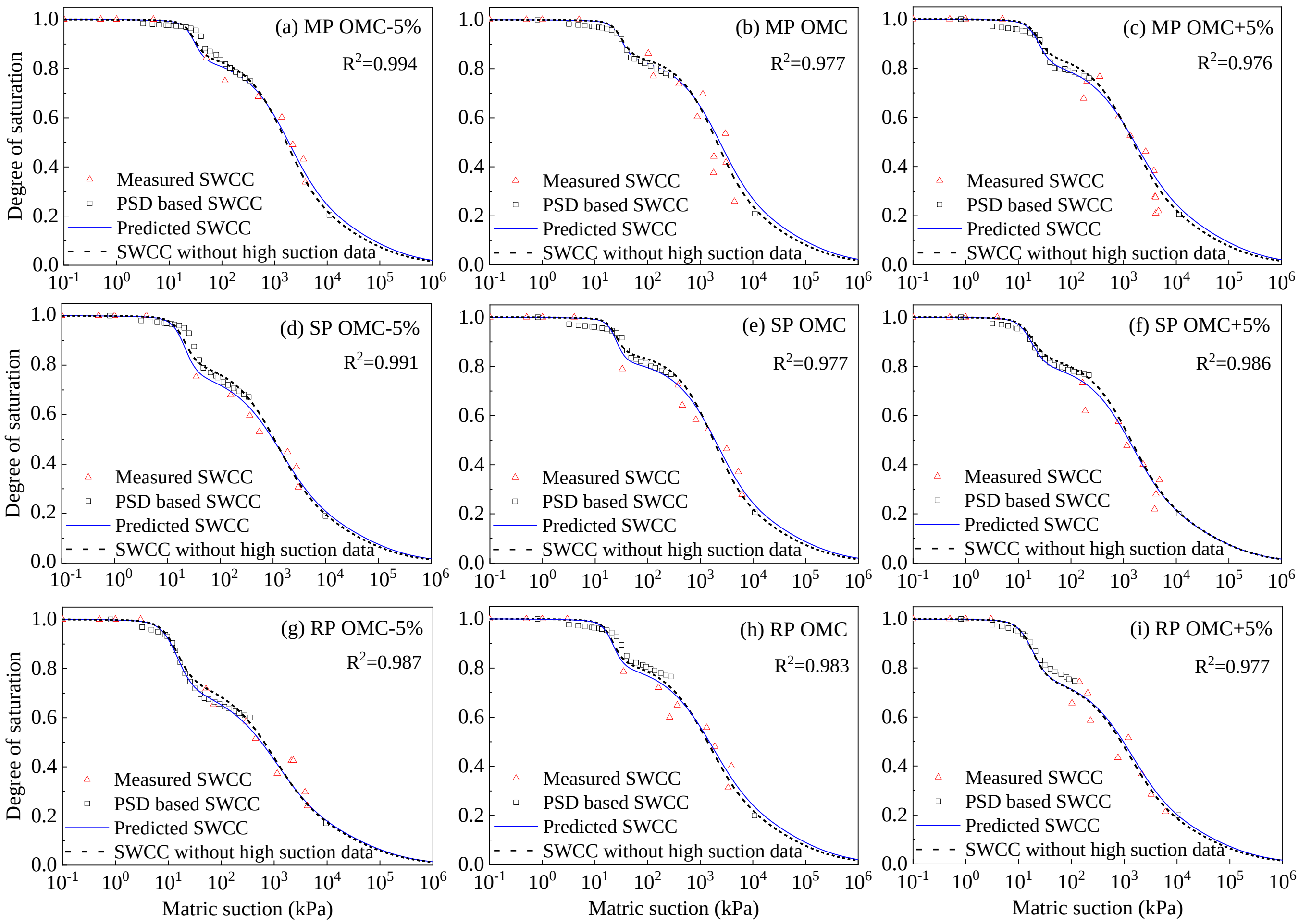

Figure 13. Prediction curves of bimodal SWCC without high suction section data.

4. Conclusions

This paper conducted a series of SWCC measurement tests and MIP tests to investigate the bimodal SWCC of fine-grained subgrade soil following an actual hydraulic path. A new determination method for bimodal SWCC was proposed that incorporated PSD data, and its efficiency was verified under nine different compaction conditions. Based on the test results, the following conclusions can be drawn:

- Based on the analysis of hydraulic paths and SWCC-PSD correlations, the SWCC of the subgrade soil should be determined to follow the actual hydraulic path.
- PSD-based SWCC fits well with the test data from the filter paper method for the low suction range corresponding to inter-aggregate pores, while it overestimates the SWCC of the medium suction range and underestimates the SWCC of the high suction range due to the inherent error of the MIP method.
- The bimodal SWCC over a wide suction range is determined by combining the filter paper method, the vapor equilibrium method for the medium and high suction range and PSD-based SWCC data for the low suction range. The prediction curves fit well with the test data.
- In the absence of high suction section data, the data obtained from PSD-based SWCC can replace the 4th turning point to predict the SWCC within the acceptable prediction error. Thus, the entire bimodal SWCC can be determined by the filter paper method and MIP test.

Author Contributions: Conceptualization, X.C.; Methodology, M.M.; Software, S.Z.; Validation, M.H.; Data curation, J.M.; Writing—original draft, S.W. All authors have read and agreed to the published version of the manuscript.

Funding: The study is funded by the National Key Research and Development Program of China (2018YFB1600201), the National Natural Science Foundation of China (U1833123), and the DOT of Jiangxi Province, China.

Data Availability Statement: Some or all of the data or code supporting the results of this study are available from the corresponding authors upon request.

Conflicts of Interest: Author Xinran Chen, Minglei Ma, Shumei Zhou, Sen Wei were employed by the China Construction Eighth Engineering Division Co., Ltd. The remaining authors declare that the research was conducted in the absence of any commercial or financial relationships that could be construed as a potential conflict of interest.

Abbreviations

SWCC	soil–water characteristic curve
PSD	pore size distribution
MIP	mercury intrusion porosimetry
GSD	grain-size distribution
OMC	optimum moisture content
MP	modified proctor
SP	standard proctor
RP	reduced proctor
RH	relative humidity

References

1. Williams, J.; Prebble, R.E.; Williams, W.T.; Hignett, C.T. The influence of texture, structure and clay mineralogy on the soil moisture characteristic. *Soil Res.* **1983**, *21*, 15–32. [CrossRef]
2. Leong, E.C.; Rahardjo, H. Review of soil-water characteristic curve equations. *J. Geotech. Geoenviron. Eng.* **1997**, *123*, 1106–1117. [CrossRef]
3. Guoquan, D.; Xia, B.; Junping, Y.; Jungao, Z. Bimodal SWCC and Bimodal PSD of Soils with Dual-Porosity Structure. *Math. Probl. Eng.* **2022**, *2022*, 4052956.
4. Zhao, Y.; Rahardjo, H.; Satyanaga, A.; Zhai, Q.; He, J. A General Best-Fitting Equation for the Multimodal Soil-Water Characteristic Curve. *Geotech. Geol. Eng.* **2023**, *41*, 3239–3252. [CrossRef]
5. Wang, J.P.; Hu, N.; François, B.; Lambert, P. Estimating water retention curves and strength properties of unsaturated sandy soils from basic soil gradation parameters. *Water Resour. Res.* **2017**, *53*, 6069–6088. [CrossRef]
6. Zhai, Q.; Rahardjo, H.; Satyanaga, A.; Dai, G. Estimation of unsaturated shear strength from soil-water characteristic curve. *Acta Geotech.* **2019**, *14*, 1977–1990. [CrossRef]
7. Mahmoodabadi, M.; Bryson, L.S. Direct application of the soil-water characteristic curve to estimate the shear modulus of unsaturated soils. *Int. J. Geomech.* **2021**, *21*, 04020243. [CrossRef]
8. Tao, R.; Cao, Z.; Pan, Y.; Najjar, S.; Medina-Cetina, Z.; Ching, J. Effects of Bimodal SWCC on Unsaturated Loess Slope Stability Analysis. *Geo-Risk* **2023**, *346*, 291–300.
9. Lu, N.; Godt, J.W.; Wu, D.T. A closed-form equation for effective stress in unsaturated soil. *Water Resour. Res.* **2010**, *46*, W05515. [CrossRef]
10. Xiao, T.; Li, P.; Pan, Z.; Hou, Y.; Wang, J. Relationship between water retention capacity and pore-size distribution of compacted loess. *J. Soils Sediments* **2022**, *22*, 3151–3165. [CrossRef]
11. Wang, K.; Hui, Y.; Zhou, C.; Li, X.; Rong, Y. Soil-water characteristic surface model of soil-rock mixture. *J. Mt. Sci.* **2023**, *20*, 2756–2768. [CrossRef]
12. Zhai, Q.; Rahardjo, H.; Satyanaga, A. Effects of residual suction and residual water content on the estimation of permeability function. *Geoderma* **2017**, *303*, 165–177. [CrossRef]
13. Brooks, R.; Corey, A. *Hydraulic Properties of Porous Media*; Hydrology Papers; Colorado State University: Fort Collins, CO, USA, 1964; Volume 3, pp. 1–27.
14. Van Genuchten, M.T. A closed-form equation for predicting the hydraulic conductivity of unsaturated soils. *Soil Sci. Soc. Am. J.* **1980**, *44*, 892–898. [CrossRef]
15. Fredlund, D.G.; Xing, A.Q. Equations for the soil-water characteristic curve. *Can. Geotech. J.* **1994**, *31*, 521–532. [CrossRef]
16. Amin, S.; Mahdieh, A.; An, D.; Taheri, A. A simplified method for determination of the soil-water characteristic curve variables. *Int. J. Geotech. Eng.* **2019**, *13*, 316–325.

17. Wang, S.J.; Fan, W.X.; Zhu, Y.Y.; Zhang, J. The effects of fitting parameters in best fit equations in determination of soil-water characteristic curve and estimation of hydraulic conductivity function. *Rhizosphere* **2020**, *17*, 100291. [CrossRef]
18. Zhai, Q.; Rahardjo, H.; Satyanaga, A.; Dai, G.; Zhuang, Y. A framework to estimate the soil-water characteristic curve for the soil with different void ratios. *Bull. Eng. Geol. Environ.* **2020**, *79*, 4399–4409. [CrossRef]
19. Satyanaga, A.; Rahardjo, H.; Leong, E.C.; Wang, J.Y. Water characteristic curve of soil with bimodal grain-size distribution. *Comput. Geotech.* **2013**, *48*, 51–61. [CrossRef]
20. Smettem, K.R.J.; Kirkby, C. Measuring the hydraulic properties of a stable aggregated soil. *J. Hydrol.* **1990**, *117*, 1–13. [CrossRef]
21. Wilson, G.V.; Jardine, P.M.; Gwo, J.P. Modeling the hydraulic properties of a multiregion soil. *Soil Sci. Soc. Am. J.* **1992**, *56*, 1731–1737. [CrossRef]
22. Burger, C.A.; Shackelford, C.D. Evaluating dual porosity of pelletized diatomaceous earth using bimodal soil-water characteristic curve functions. *Can. Geotech. J.* **2001**, *38*, 53–66. [CrossRef]
23. Wijaya, M.; Leong, E.C. Equation for unimodal and bimodal soil-water characteristic curves. *Soils Found.* **2016**, *56*, 291–300. [CrossRef]
24. Gould, S.; Rajeev, P.; Kodikara, J.; Zhao, X.L.; Burn, S.; Marlow, D. A new method for developing equations applied to the water retention curve. *Soil Sci. Soc. Am. J.* **2012**, *76*, 806–814. [CrossRef]
25. Li, X.; Li, J.H.; Zhang, L.M. Predicting bimodal soil-water characteristic curves and permeability functions using physically based parameters. *Comput. Geotech.* **2014**, *57*, 85–96. [CrossRef]
26. Gitirana, G.; Fredlund, D.G. Soil-water characteristic curve equation with independent properties. *J. Geotech. Geoenviron. Eng.* **2004**, *130*, 209–212. [CrossRef]
27. Othmer, H.; Diekkruger, B.; Kutilek, M. Bimodal porosity and unsaturated hydraulic conductivity. *Soil Sci.* **1991**, *152*, 139–150. [CrossRef]
28. Mallants, D.; Tseng, P.H.; Toride, N.; Tinunerman, A.; Jin, F.Y. Evaluation of multimodal hydraulic functions in characterizing a heterogeneous field soil. *J. Hydrol.* **1997**, *195*, 172–199. [CrossRef]
29. Zhang, L.M.; Chen, Q. Predicting bimodal soil-water characteristic curves. *J. Geotech. Geoenviron. Eng.* **2005**, *131*, 666–670. [CrossRef]
30. Ren, X.; Kang, J.; Ren, J.; Chen, X.; Zhang, M. A method for estimating soil water characteristic curve with limited experimental data. *Geoderma* **2020**, *360*, 114013. [CrossRef]
31. Atma, P.; Budhaditya, H.; Sreedeep, S. Probabilistic analysis of soil-water characteristic curve using limited data. *Appl. Math. Model.* **2021**, *89*, 752–770.
32. Zhai, Q.; Rahardjo, H.; Satyanaga, A.; Dai, G. Estimation of the soil-water characteristic curve from the grain size distribution of coarse-grained soils. *Eng. Geol.* **2020**, *267*, 105502. [CrossRef]
33. Chai, J.; Khaimook, P. Prediction of soil-water characteristic curves using basic soil properties. *Transp. Geotech.* **2020**, *22*, 100295. [CrossRef]
34. Hwang, S.I.; Lee, K.P.; Lee, D.S.; Powers, S.E. Models for estimating soil particle-size distributions. *Soil Sci. Soc. Am. J.* **2002**, *66*, 1143–1150. [CrossRef]
35. Sasanian, S.; Newson, T.A. Use of mercury intrusion porosimetry for microstructural investigation of reconstituted clays at high water contents. *Eng. Geol.* **2013**, *158*, 15–22. [CrossRef]
36. Nowamooz, H. Effective stress concept on multi-scale swelling soils. *Appl. Clay Sci.* **2014**, *101*, 205–214. [CrossRef]
37. Liu, S.Y.; Yu, J.; Yasufuku, N. Physically based soil water characteristic curves function for soils with inner porosity. *Arch. Agron. Soil Sci.* **2019**, *65*, 537–548. [CrossRef]
38. Li, H.; Li, T.L.; Li, P.; Zhang, Y.G. Prediction of loess soil-water characteristic curve by mercury intrusion porosimetry. *J. Mt. Sci.* **2020**, *17*, 2203–2213. [CrossRef]
39. Tao, G.L.; Chen, Y.; Xiao, H.L.; Chen, Q.S.; Wan, J. Determining soil-water characteristic curves from mercury intrusion porosimeter test data using fractal theory. *Energies* **2019**, *12*, 752. [CrossRef]
40. *JTG 3430-2020*; Test Methods of Soils for Highway Engineering. Research Institute of Highway Ministry of Transport: Beijing, China, 2020. (In Chinese)
41. Bittelli, M.; Flury, M. Errors in water retention curves determined with pressure plates. *Soil Sci. Soc. Am. J.* **2009**, *73*, 1453–1460. [CrossRef]
42. Nam, S.; Gutierrez, M.; Diplas, P.; Petrie, J.; Wayllace, A.; Lu, N.; Muñoz, J.J. Comparison of testing techniques and models for establishing the SWCC of riverbank soils. *Eng. Geol.* **2010**, *110*, 1–10. [CrossRef]
43. *ASTM D 6836-16*; Standard Test Methods for Determination of the Soil Water Chararcteristic Curve for Desorption Using a Hanging Column, Pressure Extractor, Chilled Mirror Hygrometer, and/or Centrifuge. ASTM International: West Conshohocken, PA, USA, 2016.
44. *ASTM D 5298-16*; Standard Test Method for Measurement of Soil Potential (Suction) Using Filter Paper. ASTM International: West Conshohocken, PA, USA, 2016.
45. Blatz, J.A.; Cui, Y.J.; Oldecop, L. Vapour equilibrium and osmotic technique for suction control. *Geotech. Geol. Eng.* **2008**, *26*, 661–673. [CrossRef]
46. Aldaood, A.; Bouasker, M.; Al-Mukhtar, M. Soil-Water Charact Curve Lime Treat Gypseous Soil. *Appl. Clay Sci.* **2014**, *102*, 128–138. [CrossRef]

47. Rajesh, S.; Khan, V. Characterization of water sorption and retention behavior of partially saturated GCLs using vapor equilibrium and filter paper methods. *Appl. Clay Sci.* **2018**, *157*, 177–188. [CrossRef]
48. Yao, Z.H.; Sun, F.X.; Fang, X.W.; Chen, Z.H. Water retention characteristics of unsaturated bentonite-sand mixtures under controlled-temperature. *Environ. Earth Sci.* **2021**, *80*, 1–15. [CrossRef]
49. Romero, E.; Simms, P.H. Microstructure investigation in unsaturated soils: A review with special attention to contribution of mercury intrusion porosimetry and environmental scanning electron microscopy. *Geotech. Geol. Eng.* **2008**, *26*, 705–727. [CrossRef]
50. Al-Mahbashi, A.M.; Elkady, T.Y.; Al-Shamrani, M.A. Hysteresis soil-water characteristic curves of highly expansive clay. *Eur. J. Environ. Civ. Eng.* **2018**, *22*, 1041–1059. [CrossRef]
51. Chen, P.; Lu, N.; Wei, C.F. General scanning hysteresis model for soil-water retention curves. *J. Geotech. Geoenviron. Eng.* **2019**, *145*, 04019116. [CrossRef]
52. Pham, H.Q.; Fredlund, D.G.; Barbour, S.L. A study of hysteresis models for soil-water characteristic curves. *Can. Geotech. J.* **2005**, *42*, 1548–1568. [CrossRef]
53. Mohamed, M.H.; Sharma, R.S. Role of dynamic flow in relationships between suction head and degree of saturation. *J. Geotech. Geoenviron. Eng.* **2007**, *133*, 286–294. [CrossRef]
54. Jayanth, S.; Iyer, K.; Singh, D.N. Influence of drying and wetting cycles on SWCCs of fine-grained soils. *J. Test. Eval.* **2012**, *40*, 376–386. [CrossRef]
55. Kristo, C.; Rahardjo, H.; Satyanaga, A. Effect of hysteresis on the stability of residual soil slope. *Int. Soil Water Conserv. Res.* **2019**, *7*, 226–238. [CrossRef]
56. Ng, C.W.W.; Sadeghi, H.; Hossen, S.B.; Chiu, C.F.; Alonso, E.E.; Baghbanrezvan, S. Water retention and volumetric characteristics of intact and re-compacted loess. *Can. Geotech. J.* **2016**, *53*, 1258–1269. [CrossRef]
57. Ding, D.; Zhao, Y.; Feng, H.; Peng, X.; Si, B. Using the double-exponential water retention equation to determine how Soil Pore-Size distribution is linked to soil texture. *Soil Tillage Res.* **2016**, *156*, 119–130. [CrossRef]
58. Xie, X.; Li, P.; Hou, X.; Li, T.; Zhang, G. Microstructure of compacted loess and its influence on the soil-water characteristic curve. *Adv. Mater. Sci. Eng.* **2020**, *5*, 1–12. [CrossRef]
59. Simms, P.H.; Yanful, E.K. Estimation of soil-water characteristic curve of clayey till using measured pore-size distributions. *J. Environ. Eng.* **2004**, *130*, 847–854. [CrossRef]
60. Seiphoori, A.; Ferrari, A.; Laloui, L. Water retention behaviour and microstructural evolution of mx-80 bentonite during wetting and drying cycles. *Géotechnique* **2014**, *64*, 721–734. [CrossRef]
61. Chen, R.P.; Liu, P.; Liu, X.M.; Wang, P.F.; Kang, X. Pore-scale model for estimating the bimodal soil-water characteristic curve and hydraulic conductivity of compacted soils with different initial densities. *Eng. Geol.* **2019**, *260*, 105199. [CrossRef]
62. Zhang, L.M.; Li, X. Microporosity structure of coarse granular soils. *J. Geotech. Geoenviron. Eng.* **2010**, *136*, 1425–1436. [CrossRef]